PAPER • OPEN ACCESS

The optical control of phase locking of polariton condensates

New Journal of Physics
The open access journal at the forefront of physics

Deutsche Physikalische Gesellschaft DPG
IOP Institute of Physics

Published in partnership with: Deutsche Physikalische Gesellschaft and the Institute of Physics

OPEN ACCESS

RECEIVED
22 February 2019

REVISED
27 September 2019

ACCEPTED FOR PUBLICATION
11 October 2019

PUBLISHED
1 November 2019

PAPER

The optical control of phase locking of polariton condensates

I Y Chestnov[1,2,3], A V Kavokin[1,2] and A V Yulin[4,5]

[1] Westlake University, School of Science, 18 Shilongshan Road, Hangzhou 310024, Zhejiang Province, People's Republic of China
[2] Westlake Institute for Advanced Study, Institute of Natural Sciences, 18 Shilongshan Road, Hangzhou 310024, Zhejiang Province, People's Republic of China
[3] Vladimir State University, Gorki St. 87, 600000, Vladimir, Russia
[4] National Research University of Information Technologies, Mechanics and Optics (ITMO University), Saint-Petersburg 197101, Russia
[5] Science Institute, University of Iceland, Dunhagi 3, 107 Reykjavik, Iceland

E-mail: igor_chestnov@westlake.edu.cn

Keywords: exciton polaritons, nonequilibrium condensates, synchronization, microcavities

Abstract

The phase and the frequency of an exciton polariton condensate excited by a nonresonant pump can be efficiently manipulated by an external coherent light. Being tuned close to the resonance with the condensate eigenfrequency, the external laser light imposes its frequency to the condensate and locks its phase, thereby manifesting a synchronization effect. The conditions of formation of the phase synchronized regime are determined. The synchronization of a couple of closely spaced polariton condensates by a spatially uniform coherent light is examined. At the moderate strength of the coherent driving the synchronization is accompanied by the appearance of symmetry-breaking states of the polariton dyad, while these states are superseded by the symmetric state at the high-intensity driving. By employing a zero-dimensional model of coupled dissipative oscillators with both dissipative and conservative coupling, we study the bifurcation scenario of the symmetry-breaking state formation.

1. Introduction

A strong light–matter interaction in semiconductor microcavities gives rise to formation of composite quasiparticles called exciton polaritons [1]. Being a superposition of excitons and photons, they provide a strong optical nonlinearity and may be characterized by a very light effective mass. These fascinating properties advantage polaritons over cold atoms in demonstrating collective many-body phenomena at high temperatures [2, 3]. However, the main difference of polaritonic systems from the conventional atomic condensates is a strong dissipation stemming from the finite lifetime of microcavity photons which necessitates external pumping to maintain polariton population.

The experimental methods for excitation of coherent polaritons may be divided into two classes: nonresonant and resonant (or quasi-resonant). The first class may be also referred to as incoherent pumping where the phase of the forming condensate does not depend on the phase of the pump. This regime is frequently realized in polariton lasers [2] that can be pumped both optically and electrically [4]. In both cases, the nonresonant pumping creates a reservoir of incoherent polaritons. If the pumping strength exceeds the threshold value, the polaritons condense to a single quantum state [5, 6]. The relaxation process is accelerated due to the bosonic stimulation by an occupancy of the final state. Note that such a spontaneous buildup of a quantum coherence is not phase-selective in the sense that the phase of the condensate is chosen spontaneously during the condensation.

When the condensation simultaneously occurs in several closely spaced condensation centers pinned to the system inhomogeneities, the interaction between condensates leads to their mutual synchronization [7, 8]. Although the total ensemble of the interacting condensates remains invariant to the global phase shift, the phase difference between neighboring condensates is locked by the coupling [9]. Besides the synchronization can also take place between different polarization components of the spinor polariton condensate in the presence of intrinsic Josephson or spin–orbit coupling (caused by the TE-TM splitting) between the polarizations [10].

It is crucial that the coupling between the driven-dissipative condensates is inherently complex, i.e. it affects not only the energy of the coupled state as the conventional conservative (Josephson) coupling typical for atomic condensates, but also the net losses [11]. Since for the driven dissipative systems the coupling is determined self-consistently with the amplitudes of the condensates [12], it is expected that several coupled condensates may be phase locked in various configurations which are characterized by different eigenfrequencies and condensation thresholds. The particular state of the ensemble is chosen during the condensation according to the selection mechanism, which favors the state with the lowest polariton lasing threshold to grow faster than the other [11]. Recently it was demonstrated that under certain conditions the steady-state configuration of an ensemble of coupled polariton condensates can be associated with the global minimum of a particular spin Hamiltonian [13, 14] assuming that the phases of the condensates are mapped to two-dimensional classical spins. The phenomenon of establishment of a mutual coherent state of several polariton condensates can be considered as a synchronization of interacting polariton lasers by analogy with the coherent dynamics of arrays of interacting lasers [15, 16].

In contrast to the nonresonant pump, the quasiresonant excitation of polaritons with a coherent light provides a reliable tool of control of their properties. Namely, polaritons are formed in the state which assumes the frequency from the pump and is phase-locked with it. In this paper we address the problem of synchronization of the coherent polariton state created by nonresonant pumping to the coherent light having frequency that is close to the frequency of the condensate. In the simplest case of a single condensate whose eigenfrequency matches the frequency of the laser light, the solution of this problem is trivial: the coherent excitation cancels the invariance to the global phase shift, thus the condensate is phase locked with the laser light [17, 18]. Here we demonstrate that even in the absence of a precise resonance, a coherent laser light is capable to impose its frequency and its phase on the condensate. Drawing an analogy with the synchronization of a dissipative oscillator by a continuous driving force [19], we consider this problem in terms of the synchronization phenomenon.

The problem under study is relevant to the recent studies of phase-locked polariton condensates aimed at the realization of polariton simulators. The manipulation of the condensate phase by the coherent light can be associated with the action of an effective magnetic field on the particular pseudo-spin. The study of the interaction of the coherent light with an ensemble of coupled condensates is important as a tool of control over phase locking in an *XY*-polariton simulator. Recently the particular case of a coherent pumping at the frequency being a multiple to the condensate eigenfrequency was considered [17]. Here, in contrast, we consider different regimes of the synchronization of the coupled polariton condensates to the external near-resonant coherent drive. Special attention is paid to the symmetry breaking bifurcation and the formation of the synchronized asymmetric states.

The paper is organized as follows. Section 2 presents the model system we consider. Section 3 describes the synchronization of a single nonresonantly excited condensate by the coherent pumping and determines the conditions of synchronization. In section 4 we extent the problem into the pair of coupled polariton condensates uniformly illuminated by the coherent light. Concluding the paper, we discuss possible implementations of the predicted phenomenon.

2. The system under study

We consider an exciton-polariton condensate excited by the incoherent pump in a planar semiconductor microcavity in the presence of the low-intensity quasi-resonant coherent laser light. The formation of the polariton condensate is described by the widely accepted mean-field model characterizing the polariton system by the complex wave function Ψ of the coherent state and by the density N_r of reservoir excitons [20]:

$$\mathrm{i}\hbar\,\partial_T\Psi = \left(-\frac{\hbar^2}{2m}(\partial_{XX}+\partial_{YY}) + g_c|\Psi|^2 + g_r N_r + \frac{\mathrm{i}\hbar}{2}(RN_r-\gamma_c)\right)\Psi + F\mathrm{e}^{-\mathrm{i}\Delta t}, \tag{1a}$$

$$\partial_T N_r = P - (\gamma_r + R|\Psi|^2)N_r. \tag{1b}$$

Here T is time, m is the polariton effective mass, the terms g_c and g_r are responsible for the energy shifts due to the polariton-polariton repulsion and the interaction with the reservoir, respectively. Populations of both condensate and reservoir dissipate with the rates γ_c and γ_r, respectively. The net dissipation is balanced by the pump P creating the incoherent excitons which then scatter to the condensate with the rate $RN_r|\Psi|^2$. The last term in the right-hand side of (1*a*) accounts for the spatially uniform coherent driving whose frequency is detuned from the bottom of the lower polariton branch by Δ.

For the sake of simplicity of the following calculations we rewrite the equations (1*a*) and (1*b*) in a dimensionless form:

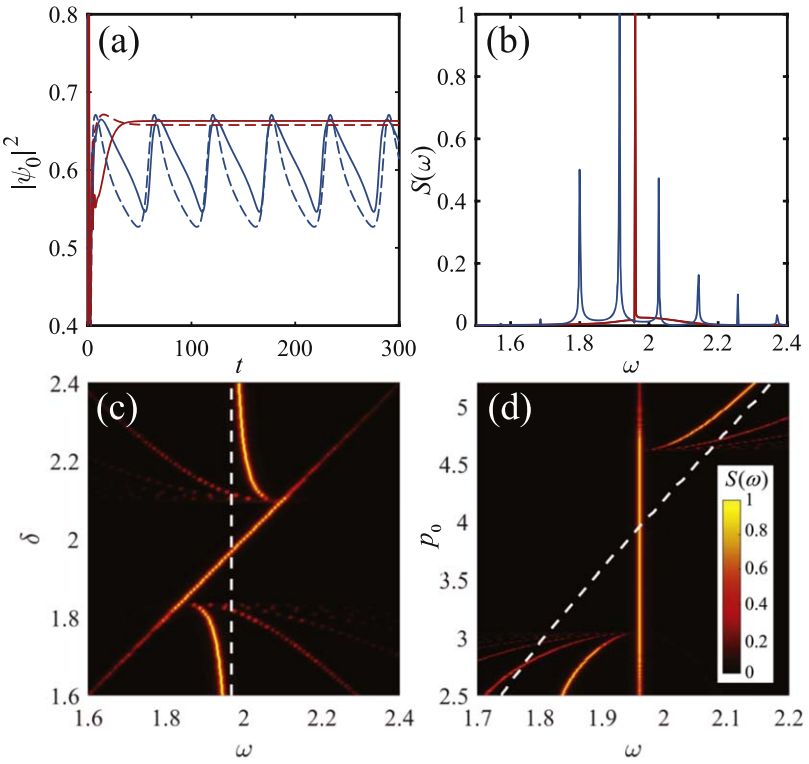

Figure 1. Synchronization of a single polariton condensate by an external coherent light. Panels (a) and (b) show, respectively, the dynamics of the condensate density maximum $|\psi_0|^2 = |\psi(\mathbf{r} = \mathbf{r}_0)|^2$ and the corresponding temporal spectra $S(\omega) = \left|\int \psi(\mathbf{r} = \mathbf{r}_0)\mathrm{e}^{-\mathrm{i}\omega t}\mathrm{d}t\right|^2$ normalized to unity. The red curves correspond to the driving frequency $\delta = 1.96$ which is close to the condensate eigenfrequency $\mu \approx 1.9604$ at $p_0 = 4$, while the blue curves correspond to the strongly nonresonant driving $\delta = 1.8$. The solid curves were calculated with use of the full model (2). The dashed curves correspond to the predictions of the simplified model (3). (c) The evolution of the condensate spectral density $S(\omega)$ as the driving frequency δ varies while the nonresonant pump amplitude is fixed to $p_0 = 4$. (d) The same as on (c) but when the amplitude of the incoherent pump p_0 varies while $\delta = 1.96$. The white dashed lines on (c) and (d) indicate the condensate eigenfrequency μ obtained at $f = 0$. For all panels $g = 0.46, \beta = 2.5, \gamma = 0.4, f = 0.07$ and $l = 0.93$.

$$\mathrm{i}\partial_t\psi = \left(-\frac{1}{2}(\partial_{xx} + \partial_{yy}) + \mathrm{i}(n_r - 1) + |\psi|^2 + gn_r\right)\psi + f\mathrm{e}^{-\mathrm{i}\delta t}, \tag{2a}$$

$$\partial_t n_r = p - (\gamma + \beta|\psi|^2)n_r, \tag{2b}$$

where we have redefined $t = T\gamma_c/2$, $x = X\sqrt{m\gamma_c/2\hbar}$, $y = Y\sqrt{m\gamma_c/2\hbar}$, $\psi = \Psi\sqrt{2g_c/\hbar\gamma_c}$, $n_r = RN_r/\gamma_c$, $g = 2g_r/\hbar R$, $\gamma = 2\gamma_r/\gamma_c$, $\beta = \hbar R/g_c$, $p = 2RP/\gamma_c^2$, $f = F\sqrt{8g_c/\hbar\gamma_c^3}$ and $\delta = 2\Delta/\gamma_c$.

3. Synchronization of a single polariton condensate by a coherent laser light

We start considering the interaction of a single polariton condensate with the external coherent light. We assume that the nonresonant pump has a Gaussian shape $p(\mathbf{r}) = p_0 \exp\left(-\frac{(\mathbf{r}-\mathbf{r}_0)^2}{2l^2}\right)$, where $\mathbf{r}$ is an in-plane vector. In the absence of the resonant excitation the condensate is formed in the steady state $\psi(\mathbf{r}, t) = \psi(\mathbf{r})\exp(-\mathrm{i}\mu t)$ provided that the incoherent pump amplitude p_0 exceeds the threshold. Here μ is the condensate chemical potential. In the framework of the mean-field model (2), the spontaneous choice of the condensate phase which can be parameterized as $\varphi = \arg(\psi(\mathbf{r} = \mathbf{r}_0))$ is provided by tacking a white noise distribution of the polariton field at the initial moment of time.

As the coherent laser pumping is switched on, it tends to impose its frequency and phase on polaritons. However, the weak driving is unable to do this if the frequency mismatch between the laser and the condensate is large. Instead, it perturbs the condensate steady state inducing oscillations of polariton density—see the blue curve in figure 1(a). These oscillations can be detected by the frequency comb in the temporal spectrum of the condensate (see figure 1(b)). They are governed by the nonlinear mixing of the condensate eigenfrequency μ and the driving frequency δ.

As the driving frequency approaches (but not yet matches) the frequency of the unperturbed condensate, the steady state restores, see the red curve in figure 1(a). In this case the condensate frequency merges with the

frequency of the coherent pump manifesting itself the synchronization between the condensate and the light, see the red line in figure 1(b). Note that the merging of the spectral lines happens regardless of whether the coherent pump is tuned below or above the condensate frequency. Indeed, the range of the driving frequencies providing synchronization is shown in figure 1(c), which illustrates the evolution of the condensate spectrum as the driving frequency δ scans from the red-detuned to the blue-detuned region, while the driving amplitude f remains fixed. Those states whose spectrum consists of a single line are synchronized with the external light.

The spectral width of the synchronization domain is dependent on f as well as on the properties of the condensate. For instance, the variation of the amplitude of the incoherent pump p_0, that corresponds to the variation of the condensate eigenfrequency μ, also reveals synchronization in the finite range of pumping amplitudes, see figure 1(d).

The above discussion stems from the numerical analysis of (2). To achieve analytical results and to explain the synchronization phenomenon in simple terms we simplify model (2) by substituting it with a single ordinary differential equation for the complex amplitude A of the polariton field:

$$\mathrm{i}\partial_t A = (\alpha|A|^2 - \tilde{\delta} + \mathrm{i}\Gamma - \mathrm{i}\nu|A|^2)A + \tilde{f}, \tag{3}$$

which was written in the reference frame rotating with the effective driving frequency $\tilde{\delta}$. Here we have introduced the net gain Γ, the saturation of the gain $\nu|A|^2$ accounting for the effect of the reservoir depletion, the effective nonlinear frequency shift α and the effective driving force $\tilde{f}$. The correspondence between the parameters of the model (2) and their counterparts in (3) is discussed in appendix A.

Equation (3) is relatively easy to analyze. In the absence of the coherent pump, the steady state solution reads: $A = \sqrt{n_0}\exp(-\mathrm{i}\mu_0 t)$, where $n_0 = \Gamma/\nu$ and $\mu_0 = \alpha n_0 - \tilde{\delta}$ corresponds to the frequency mismatch between the driving force and the condensate eigenfrequency in the rotating frame. In the presence of the coherent pump the only possible steady state is characterized by the eigenfrequency equal to the driving frequency, $\mu_0 = 0$. Thus seeking the solution in the form $A(t) = \sqrt{n}\exp(\mathrm{i}\varphi(t))$ and assuming weakness of the coherent pump in the sense that it does not affect the condensate amplitude, $n = n_0$, we get

$$\sqrt{n_0}\,\partial_t\varphi = (\tilde{\delta} - \alpha n_0)\sqrt{n_0} - \tilde{f}\cos(\varphi). \tag{4}$$

The stable stationary solution of this equation, $\partial_t\varphi = 0$, corresponds to the establishment of the synchronization regime. It requires

$$\tilde{f} \geqslant |\tilde{\delta} - \alpha\Gamma/\nu|\sqrt{\Gamma/\nu}. \tag{5}$$

This simple synchronization condition defines the critical value of the driving strength necessary to slave the condensate. It implies that in the case of the weak driving, the synchronization occurs either in the vicinity of the resonance, $\tilde{\delta} = \alpha\Gamma/\nu$, or close to the condensation threshold where the condensate occupancy Γ/ν is low. In the close proximity of the threshold, $\Gamma/\nu \to 0$, the condensate can not resist synchronization even if the driving is weak and strongly detuned. Besides, equation (5) indicates that the synchronization condition is insensitive to the sign of the frequency mismatch.

A strict analysis of the synchronized (steady-state) solution of equation (3) yields the following equation for the condensate density:

$$(\alpha n - \tilde{\delta})^2 n + (\Gamma - \nu n)^2 n = \tilde{f}^2, \tag{6}$$

which may have either one or three real roots. Let us note that this approach accounts for the influence of the coherent pump on the amplitude of the condensate and thus is more general than the approach used in (4).

The typical shape of the $n(\tilde{f})$-dependence is shown in figure 2(a). Although the steady-state solutions exist for any value of the driving strength, the synchronous regime is established only for those states which are stable against small perturbations. The analysis of the Lyapunov exponents yields that the synchronized solution is stable, provided that

$$2\nu n > \Gamma, \tag{7a}$$

$$3(\alpha^2 + \nu^2)n^2 - 4(\Gamma\nu + \alpha\tilde{\delta})n + \tilde{\delta}^2 + \Gamma^2 > 0. \tag{7b}$$

These conditions are simultaneously satisfied for the upper branch of the S-shaped curve (see the blue curve in figure 2(a)). However at the left folding point $\tilde{f} = \tilde{f}_{b1}$ the solution becomes unstable and at $\tilde{f} < \tilde{f}_{b1}$ the synchronized state transforms into a state with two incommensurable frequencies. Mathematically it means that the pair of stable and unstable fixed points corresponding to the upper and the intermediate branches of the S-shaped curve collide at $\tilde{f} = \tilde{f}_{b1}$ and disappear giving birth to a stable limit cycle. The birth of the limit cycle manifests itself in the spectral frequency comb shown in figure 1(b).

Note that the lower branch of the S-shaped curve does not support synchronization for arbitrary small values of the driving strength as it is typically unstable in a stark contract with the conventional optical bistability regime [21], that is realized in the absence of the incoherent pumping. In particular, the whole of the lower branch is unstable provided that $\Gamma > 2\nu n_{b2}$ (see the condition (7a)), where n_{b2} determines the condensate

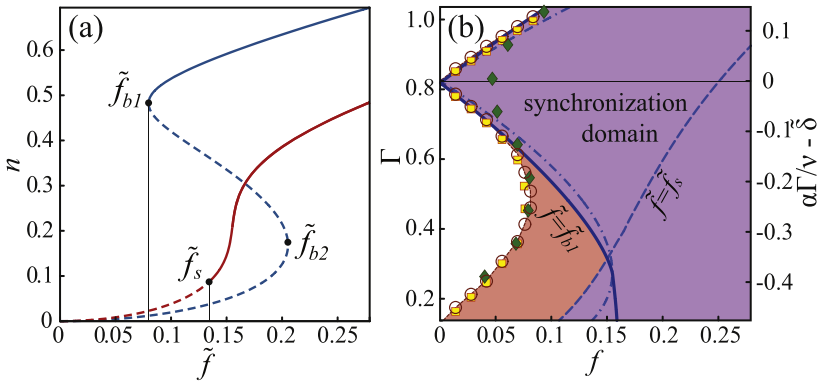

Figure 2. (a) The $n(\tilde{f})$-dependence of the steady-state solution of (3). The stable states corresponding to the synchronization with the coherent light are shown with solid curves while the dashed curves indicate unstable solutions. The gain parameter is $\Gamma = 0.6$ for the blue curve and $\Gamma = 0.24$ for the red curve. (b) The phase diagram for the synchronization of a single polariton condensate with the coherent light. The purple (dark) region corresponds to the synchronization domain predicted by the toy model (3). The red (light) region framed by the red circles is obtained from the numerical solution of the full system (2). The simplified synchronization condition (5) is shown with the dash-dotted curve. The yellow squares show the boundary of the synchronization domain under the homogeneous illumination of the symmetric polariton dyad (the interspot distance is $d = 17$, see figure 3(a)), while the green diamonds indicate the same for the antisymmetric dyad ($d = 14$). For all data $\delta = 1.96$. The rest parameters for both panels are the same as in figure 1.

density at the right bending point, see figure 2(a). In this case, the position of the left bending point $\tilde{f}_{b1}$, which can be easily obtained from (6) taking $\partial_n \tilde{f} = 0$, should be considered as the critical value of the coherent pump amplitude above which the synchronization occurs.

If equation (6) admits a single real solution (see the red curve in figure 2(a)), the inequality (7*b*) always holds and the stability of the synchronized state is governed by the condition (7*a*). Thus, the solution is also unstable at the weak driving strength, when the steady state condensate population n vanishes. However the condensate becomes stable through a supercritical Hopf bifurcation at $\tilde{f} \geqslant \tilde{f}_s$ manifesting establishment of the synchronization regime. The critical driving strength $\tilde{f}_s \equiv \tilde{f}(n_s)$ is determined from (6) taking $n = n_s = \Gamma/2\nu$.

The inequalities $\tilde{f} > \tilde{f}_s(\tilde{\delta})$ and $\tilde{f} > \tilde{f}_{b1}(\tilde{\delta})$ constitute the synchronization conditions which are shown in the phase diagram figure 2(b) plotted on the parameter plane (Γ, f). Note that the simplified condition (5) describes the synchronization phenomenon well enough, especially in the vicinity of the resonance, $\alpha\Gamma/\nu = \tilde{\delta}$, see the dash-dotted curve.

For the sake of comparison, the results of numerical simulations of the full 2D model (2) are also shown in the phase diagram, figure 2(b), see the red circles indicating the boundary of the synchronization domain. The best coincidence between the models is achieved in the vicinity of the resonance. However the region close to the condensation threshold is worse described by the toy model (3) since it factors out the reservoir-induced blue shift. The blue-shift is accounted for in the effective detuning $\tilde{\delta}$ (see appendix A). Far from the threshold, this assumption is justified by the effect of depletion of the reservoir. Indeed, if $\beta|\psi|^2 \gg \gamma$, the reservoir density $n_r = p/(\gamma + \beta|\psi|^2)$ is depleted. In contrast, if the condensate density $|\psi|^2$ is comparable to or lower than γ/β, the impact of the reservoir-induced blue shift is crucial. As a result, the simplified model overestimates the value of the frequency mismatch $\alpha\Gamma/\nu - \tilde{\delta}$ near the threshold shifting the boundary of the synchronization domain towards the higher values of the driving strength, see figure 2(b).

4. Polariton dyad in the presence of a coherent laser light

4.1. Synchronization of the symmetric and antisymmetric polariton dyad to the coherent light

Another fundamental question is what happens when not a single but several neighboring condensates are illuminated by a coherent laser light. We proceed considering the simplest case of a polariton dyad created by two spatially separated spots of the incoherent pump. In particular, we take $p(\mathbf{r}) = p_1 \exp\left(-\frac{(\mathbf{r}-\mathbf{r}_1)^2}{2l_1^2}\right) + p_2 \exp\left(-\frac{(\mathbf{r}-\mathbf{r}_2)^2}{2l_2^2}\right)$, with $d = |\mathbf{r}_1 - \mathbf{r}_2|$ being the interspot distance. Because of the outflow of polaritons from under the pump spots, the condensates interact with each other. In the absence of the coherent pump this coupling causes the formation of a mutually synchronized (coherent) state. If the pumps are identical ($p_1 = p_2$ and $l_1 = l_2$), polaritons may condense either in in-phase (symmetric) or in anti-phase (antisymmetric) configurations depending on the mutual coupling strength, which is governed by the interspot distance d and the velocity of the polariton outflow [9]. In particular, the symmetric and antisymmetric states alternate as the interspot distance varies while the nonresonant pump power remains fixed, see figure 3(a). Note that in both possible configurations the condensates are equally populated. For the

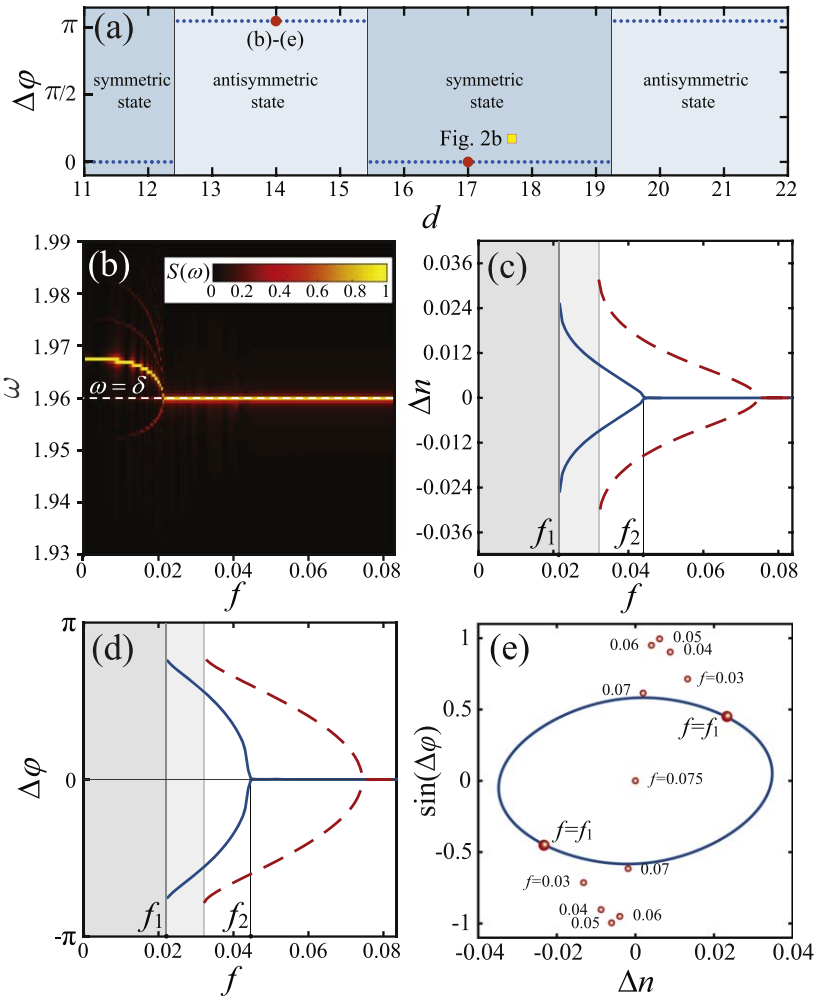

Figure 3. Synchronization of the polariton dyad with the coherent laser light. (a) Switching between the symmetric and antisymmetric states of the dyad with the growth of the inter-condensate distance d for the fixed amplitude of the incoherent pump power, $p_0 = 4$. (b) The condensate spectral density $S(\omega)$ calculated at $\mathbf{r} = \mathbf{r}_2$ from the numerical simulations of the dynamics of the full model (2) with $d = 17$. The frequency comb at low f indicates the presence of the asynchronous regime. Panels (c) and (d) show the dependencies of the steady state population imbalance Δn and the phase difference $\Delta\varphi$ on the coherent pump amplitude f, respectively. The blue solid curves correspond to the numerical solution of the full model (2) while the red dashed curves show the predictions of the equations (8*a*) and (8*b*). (e) The blue line shows the limit cycle trajectory on the $(\Delta n,\ \sin(\Delta\varphi))$ plane in the close proximity of the bifurcation point $f = f_1$. Large red points correspond to the steady-state solutions exactly at the bifurcation point. Stable symmetry broken states, which appear at $f \in [f_1, f_2)$, are shown with small points. The parameters are: $p_0 = 4, \delta = 1.96, g = 0.46, \beta = 2.5, \gamma = 0.4$ and $l_1 = l_2 = 0.93$.

sake of simplicity we leave out of the scope of this paper the class of symmetry broken solutions which appear in the weak lasing regime [11].

The external coherent driving tends to lock phases of the condensates. Hence it may alter the structure of the dyad. In this paper we focus on the case of a uniform illumination assuming that the coherent light excites the microcavity at the normal incidence. Experimentally this is feasible with strongly defocused laser beam.

We start analyzing the synchronization scenario in the framework of the full model (2). It is anticipated, that, by analogy with the case of a single condensate, a weak driving is unable to synchronize the dyad. At the same time, an intense coherent driving should dominate over the inter-condensate coupling suppressing the intrinsic structure of the dyad and synchronizing both condensates. However, the behavior at the intermediate strength lacks of understanding. Nevertheless, it is obvious that the particular synchronization scenario should depend on whether the dyad is symmetric or antisymmetric in the absence of the coherent light.

When the nonresonant pump provides the in-phase configuration of the polariton dyad (dark domains in figure 3(a)), the synchronization scenario is pretty much the same as for a single condensate although the synchronization conditions in this case are slightly affected by the inter-condensate coupling, see the yellow squares in figure 2(b). Indeed, in the absence of the coherent pump, the coupling alters the frequency of the dyad and the amplitudes of the condensates in respect to the case of a stand-alone polariton condensate. Since the dyad state remains symmetric for any value of the driving amplitude (the condensates are in-phase and equally populated both in synchronous and asynchronous regimes), the symmetric dyad can be associated to a single

driven oscillator which effective frequency and the loss rate are affected by the complex inter-condensate coupling.

The case of the condensates phase locked with π-phase difference in the absence of the coherent light is much richer. The typical synchronization scenario for this case is illustrated in figures 3(b)–(e). The weak driving induces oscillations of the condensate amplitude, see figure 3(b). From symmetry reasons, it is obvious that the antisymmetric state cannot be synchronized by the homogeneous driving without modification of the entire structure of the solution. Instead, it is anticipated that the a pair of identical condensates illuminated by the homogeneous coherent pumping should be synchronized in the symmetric state.

However, it appears that, as the coherent driving strength increases above the critical value f_1 defined in figures 3(c), (d), the limit cycle, which corresponds to the oscillating regime, is superseded by the steady state with *broken symmetry*. Despite of the fact that the incoherent pump spots are identical, the condensates have different populations and their relative phase equals neither 0 or π (see figures 3(c) and (d)).

With the further increase of the coherent pump amplitude, the degree of asymmetry of the state, i.e. the population imbalance $\Delta n = n_1 – n_2$ and the phase difference $\Delta\varphi = \varphi_1 – \varphi_2$, decrease. Here $n_{1,2} \equiv n(\mathbf{r} = \mathbf{r}_{1,2})$ and $\varphi_{1,2} \equiv \varphi(\mathbf{r} = \mathbf{r}_{1,2})$. Both Δn and $\Delta\varphi$ vanish at $f = f_2$ as a second bifurcation happens and the symmetric steady state forms, see figures 3(c) and (d). In this regime, the coherent pump dominates over inter-condensate interactions and governs the phase configuration of the dyad.

4.2. Synchronization scenario in terms of the coupled oscillators model

To study the synchronization scenario in more details we again resort to the simplified model considering the interacting condensates as a pair of linearly coupled oscillators:

$$\mathrm{i}\partial_t A_1 = (\alpha|A_1|^2 - \tilde{\delta} + \mathrm{i}\Gamma - \mathrm{i}\nu|A_1|^2)A_1 + \sigma A_2 + \tilde{f}, \tag{8a}$$

$$\mathrm{i}\partial_t A_2 = (\alpha|A_2|^2 - \tilde{\delta} + \mathrm{i}\Gamma - \mathrm{i}\nu|A_2|^2)A_2 + \sigma A_1 + \tilde{f}. \tag{8b}$$

We assume that the coupling parameter is complex, $\sigma = \sigma_\mathrm{J} + \mathrm{i}\sigma_\mathrm{d}$. The conservative (Josephson) coupling σ_J results in the frequency splitting between the symmetric and antisymmetric states. The σ_d component is responsible for the dissipative coupling which accounts for the fact that the net losses of the coupled state do depend on the relative phase. The numerical values of these parameters are obtained by fitting of the results of the simulations of the full 2D model (2) to the results predicted by the ordinary differential equations (8*a*) and (8*b*). The details of this fitting procedure are presented in appendix A.

In what follows we focus on the case of the antisymmetric polariton dyad which corresponds to the positive dissipative coupling parameter, $\sigma_\mathrm{d} > 0$. The synchronization scenario for this case, predicted by model (8*a*) and (8*b*), is shown in figure 3 with the red dashed lines while the predictions of the full model (2) correspond to the blue solid curves. Although the simplified model fails predicting the position of the bifurcation points $f_{1,2}$ accurately, both the spontaneous symmetry breaking phenomenon and the break of the synchronous regime are reproduced qualitatively correctly. Thus we believe that the analysis of the simplified model is capable to describe the behavior of the full system. The discrepancy between the models should be attributed to the renormalization of the coupling parameter σ by the presence of the homogeneous driving. Indeed, the coupling strength is determined by the interference of the overlapping condensate wave functions. An intensive homogeneous resonant pumping modifies the distribution of the condensate phase affecting thereby the overlap between neighboring condensates and altering the coupling parameter.

The spontaneous symmetry breaking scenario, which is realized as the pump intensity decreases below $f = f_2$, indicates the presence of a supercritical pitchfork bifurcation. This statement can be proved in terms of the coupled oscillators model (8*a*) and (8*b*) applying a perturbation theory in the vicinity of the bifurcation point f_2. The details of the calculations are accumulated in appendix B. In the leading order of approximation the deviation $\Delta A_{1,2}$ of the symmetry broken solution (A_1, A_2) from the symmetric one can be found in the form $\Delta A_{1,2} = a(\xi_{1,3} + \mathrm{i}\xi_{2,4})$ where $\xi_{1,2,3,4}$ are real constants defined in appendix B. The equation for the amplitude a has the form

$$\partial_t a = \lambda a + \epsilon a^3 \tag{9}$$

with real coefficients λ and ϵ. Equation (9) is the normal form of a pitchfork bifurcation. Calculation of the coefficients entering (9) yields $\epsilon < 0$. So, the symmetry breaking indeed goes through supercritical pitchfork bifurcation.

The analysis of the dynamics predicted by the coupled oscillators model reveals that the bifurcation switching the system between the synchronous and asynchronous (oscillating) regimes at $f = f_1$ is an infinite-period bifurcation, which consists in the appearance of the two pairs of stable and unstable states on the limit cycle. It destroys the motion around the limit cycle trajectory and the system switches to the one of the two stable fixed points corresponding to the solutions with broken symmetry. The limit cycle trajectory in the vicinity of

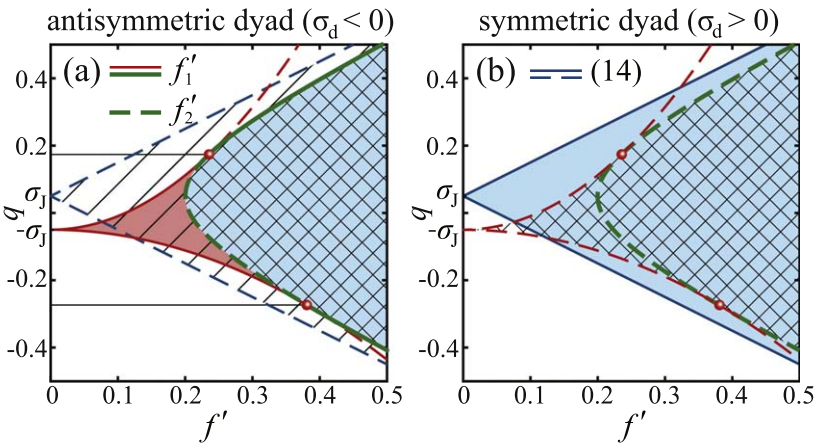

Figure 4. Bifurcation diagram of the stationary solutions of the coupled phase oscillators model (10). (a) For $\sigma_d = -0.1$ and $\sigma_J = 0.05$. (b) For $\sigma_d = 0.1$ and $\sigma_J = 0.05$. The shaded domains correspond to the stable solutions: the blue one to the symmetric state and the red one to the symmetry broken states. The regions where the dynamically unstable states exist are hatched. The diagonal hatch corresponds to the unstable symmetric solutions and the square hatch to the unstable symmetry broken states. The solid segments of the curves indicate the threshold driving f_1' required for synchronization. The red line corresponds to condition (11). Its segments bounded by the red points (between black horizontal lines) indicate the threshold driving above which a couple of symmetry broken states exist. The green line corresponds to condition (13). Its dashed segments on (a) bounded by the red points indicate the position of the pitchfork symmetry breaking bifurcation, $f' = f_2'$. The solid segments correspond to the critical value of the driving strength above which the symmetric states are dynamically stable. In both panels, the unstable symmetry broken states exist in the region on the right from the green curve. The blue lines show the boundary of existence of the symmetric solutions given by (14). Black horizontal lines determine the boundary of validity of condition (12).

the bifurcation point calculated with the coupled oscillators model is shown in figure 3(e). The large red dots on the phase trajectory mark the position the stable fixed points at $f = f_1$.

Note that the described synchronization scenario is robust against the change of the domain of the inter-condensate distances d which provide the antisymmetric configuration of the undriven dyad, see figure 3(a). However the threshold value f_1 of the coherent pump intensity corresponding to the establishment of the synchronous regime (see the green diamonds in figure 2) is sensitive to the system parameters. In particular, it depends on the frequency mismatch between the coherent driving and the condensate and on the distance d which governs the inter-condensate coupling. Besides, in the case of a strong frequency mismatch, the spontaneous symmetry breaking bifurcation and the bifurcation accompanying formation of the synchronous state merge. In this case the symmetry broken state disappears and the oscillating regime, typical for the weak coherent pumping, is directly superseded by the symmetric state, $\Delta = 0$, as the driving strength increases above f_2. In order to determine the conditions of existence of the symmetry broken state, we further simplify the coupled oscillators model reducing it to the model of symmetrically driven coupled phase oscillators.

4.3. Coupled phase oscillators model

By analogy with the case of a single oscillator (4), we assume that the driving strength is weak and does not affect the condensate populations, $|A_1| = |A_2| = \sqrt{\Gamma/\nu}$. Thus, taking $A_{1,2} = |A_{1,2}| \exp(\mathrm{i}\varphi_{1,2})$, the state of the dyad is described by the coupled equations for the condensate phases:

$$\partial_t \varphi_{1,2} = q - \sigma_J \cos(\varphi_{2,1} - \varphi_{1,2}) + \sigma_d \sin(\varphi_{2,1} - \varphi_{1,2}) - f' \cos\varphi_{1,2}, \tag{10}$$

where $q = \tilde{\delta} - \alpha\Gamma/\nu$ is an effective detuning and $f' = \tilde{f}\sqrt{\nu/\Gamma}$. In the absence of the driving, $f' = 0$, these equations predict the formation of the symmetric state $\varphi_2 - \varphi_1 = 0$ at positive dissipative coupling $\sigma_d > 0$ and the antisymmetric state $\varphi_2 - \varphi_1 = \pi$ at $\sigma_d < 0$.

Being quite simple, model (10) predicts the same synchronization scenario as observed in 2D case. In particular, equations (10) have both symmetric $\varphi_1 = \varphi_2$ and the symmetry broken $\varphi_1 \neq \varphi_2$ stationary solutions, see appendix C. The corresponding bifurcation diagram is shown in figure 4.

The analysis shows that the solution with broken symmetry appears provided that the coherent driving strength exceeds the threshold value, which is defined as

$$f_1' = 2(\sqrt{(\sigma_J + q)^2(\sigma_J^2 + \sigma_d^2)} - \sigma_J(\sigma_J + q))^{1/2} \tag{11}$$

at the detuning q belonging to the range

$$|q + \sigma_J| < 2\sqrt{\sigma_J^2 + \sigma_d^2}. \tag{12}$$

Although the stationary solutions with broken symmetry exist at any value of the complex coupling, for the dyad which is symmetric at zero driving (i.e. at $\sigma_d > 0$) they are always dynamically unstable and hence can not be observed experimentally. In contrast, the antisymmetric dyad ($\sigma_d < 0$) can transform into the stable symmetry broken states. Moreover, it can happen even at vanishing driving strength provided that its frequency matches the eigenfrequency of the stand-alone dyad, namely, at $q = -\sigma_J$, see (11) and figure 4(a). In the latter case the symmetry broken state bifurcates from the antisymmetric solution $\varphi_2 - \varphi_1 = \pi$ at $f' = 0$. With the increase of the driving strength the degree of asymmetry of the state, i.e. the phase difference $\varphi_2 - \varphi_1$, decreases until the symmetry broken states disappear at the pitchfork bifurcation (which is of supercritical type at $\sigma_d < 0$ and of subcritical type in the opposite case) at $f' = f'_2$, where:

$$f'_2 = \sqrt{4\sigma_d^2 + (q - \sigma_J)^2}. \tag{13}$$

Note that the stable symmetry broken solutions do not appear at any driving strength if condition (12) violates, i.e. if the laser frequency is strongly detuned from the eigenfrequency of the stand-alone antisymmetric dyad. Although there are other symmetry broken solutions, which exist at $f' > f'_2$ for arbitrary detuning, these states are always dynamically unstable (see appendix C for the details). In figure 4 these solutions lie on the right from the green curve.

Besides the symmetry broken solutions, there are also the symmetric states which appear provided that

$$f' > |q - \sigma_J|. \tag{14}$$

At $\sigma_d > 0$ there is a pair of symmetric solutions which are always stable. Both these states have the same frequency inherited from the coherent driving but different phase shifts in respect to the laser light phase. In this case condition (14) determines the synchronization threshold and is equivalent to (5).

In the case of the dyad which is antisymmetric at zero driving ($\sigma_d < 0$), the symmetric synchronized states become stable only at $f' > f'_2$, see the blue shaded region in figure 4(a). Thus the synchronization of the antisymmetric dyad typically requires much stronger power than in the symmetric case.

Note that the domains of existence of the synchronized solutions defined by the conditions (11)–(14) remain invariant to the change of a sign of the dissipative coupling σ_d. However, the stability properties of the solutions are different for the symmetric and the antisymmetric dyad as figure 4 shows. Besides, the change of a sign of the Josephson coupling σ_J leads to the reflection of the bifurcation diagram about $q = 0$ axis. Note that both dissipative and Josephson coupling parameters varies with the variation of the inter-condensate distance and the pumping power, see e.g. [9, 22].

5. Conclusion and outlook

We describe a novel mechanism of manipulation of nonequilibrium condensates of exciton polaritons formed in semiconductor microcavities. This mechanism, based upon a very general nonlinear effect of synchronization with an external coherent driving, paves the way to the nonresonant control of the properties of driven-dissipative polariton condensates. In particular, in the synchronization regime the frequency of the polariton condensate does not depend on the intensity of the incoherent pump but is equal to the coherent pump frequency. The phase of the polariton condensate is locked to the phase of the coherent pump. Thus, this effect allows to control the phase of the condensate by the detuned external laser beam. A simple model describing the spatially distributed condensate by its amplitude can qualitatively reproduce the discussed phenomena.

The interplay of mutual synchronization of a couple of neighboring condensates and their synchronization to the external coherent light is also studied. Those condensates which are locked in-phase in the absence of the coherent driving, can be easily synchronized to the coherent light. However, the synchronization of the antisymmetric polariton dyad is accompanied by the appearance of the symmetry broken configuration of neighboring polariton condensates which mediates the formation of a mutual coherent state. This intermediate regime is characterized by the imbalance of the condensate populations and corresponds to the spontaneous breaking of the state symmetry. It is superseded by the symmetric (in-phase) configuration of the polariton dyad as the intensity of the coherent light grows. The obtained results can be straightforwardly generalized to the case of an ensemble of coupled polariton condensates using the model of driven coupled dissipative oscillators.

In spite of the fact that the properties of the polariton dyad are dependent of the spatial overlap of the condensate wave functions, the model of two coupled nonlinear oscillators driven by an external force are capable to describe all the peculiarities of the synchronization scenario. Thus the model of coupled oscillators represents an effective tool for investigation of the polariton dynamics. In particular, it assists the analysis of the bifurcations happening in the polariton systems. In our case it allows to reduce the spontaneous symmetry breaking bifurcation to the normal form of a supercritical pitchfork bifurcation.

Synchronization of a single condensate by the coherent light may assist an experimental measurement of the relative phases between the condensates in the ensemble created by the multi-spot nonresonant pumping.

Fixing the phase of a single condensate one may use the quasi-resonant laser light as a reference beam. Besides, it is worth mentioning that the effect of synchronization can potentially be used for manipulation of the spin-polarized polariton condensates which are created by the polarized nonresonant laser pumping. In particular, it has been recently demonstrated [23] that the spin-up and spin-down components having different eigenfrequencies can be mutually synchronized due to spin-orbit interaction. The approach developed in the present paper can be used for the studies of how these vector polariton states can be synchronized to coherent pumps of different polarizations and frequencies.

We also believe that the effect of synchronization can assist to control the distribution of phases and amplitudes in the arrays of polariton condensates which can be useful, for example, for the engineering of polariton lasing systems consisting of polariton laser arrays and for polariton simulators. In particular, since the external coherent pump affects the condensate phase, it can be associated with the effective magnetic field [17] acting either on a single effective spin or on the several condensates in the array.

Acknowledgments

This work is supported by Westlake University (Project No. 041020100118). AVY was financially supported by the Government of the Russian Federation (Grant 074-U01) through ITMO Fellowship schemes. IYC acknowledges the support from RFBR, grants No. 17-52-10006, 17-42-330928 and the Ministry of Education and Science of the Russian Federation, Project No. 16.112 3.2017/4.6.

Appendix A. Derivation of the simplified zero-dimensional model of synchronization

The toy models (3) and (8*a*), (8*b*) are capable to explain all the peculiarities of the synchronization phenomenon. However, the quantitative agreement with the full partial differential equations (2) requires the correct values of the system parameters. In general, these parameters can be determined integrating out spatial degrees of freedom. Instead of approximating the condensate wave function and calculating overlap integrals [12], we resort to fitting of parameters of the simplified models using the predictions of the full model as a reference. The good agreement between the predictions of the simplified and full models shown in figure 2(b) justifies our approach.

The polariton field amplitude A entering the simplified models is associated with the polariton density maximum. Namely, $A = \psi_0 = \psi(\mathbf{r} = \mathbf{r}_0)$ for the single oscillator model and $A_{1,2} = \psi(\mathbf{r} = \mathbf{r}_{1,2})$ for the coupled oscillators model.

For the model (3) the effective linear gain Γ is related to the amplitude of the incoherent pump by the relation $\Gamma = b_1 p_0 - b_2$, where b_1 and b_2 can be found from the growth rate of the polariton density at the linear stage of the condensate formation and from the incoherent pump threshold, respectively. For the considered parameters (see the caption of figure 1) we obtain $b_1 = 0.237$ and $b_2 = 0.116$. The nonlinear saturation of the gain ν and the nonlinear frequency shift α are obtained fitting the dependencies of the condensate density maximum $|\psi_0|^2$ on the pump amplitude p_0 (figure A1(a)) and of the condensate eigenfrequency μ on the density maximum $|\psi_0|^2$ (figure A1(b)), respectively. The best fit is achieved for $\alpha = 0.957$ and $\nu = 1.378$. The effective driving force $\tilde{f}$ is related to the amplitude of the coherent pump as $\tilde{f} = kf$, where the factor k is obtained from the fit of the width of the synchronization domain, figure 2(b). For the considered parameters we get $k = 1.1$.

Note that the model (3) excludes the excitonic reservoir from the consideration. However, the reservoir is responsible for the blue shift of the condensate eigenfrequency, which may be significant even at the condensation threshold. At the same time, the synchronization condition is crucially affected by the detuning of the coherent light frequency from the condensate eigenfrequency. Thus the reservoir-induced frequency shift has to be taken into account in model (3). For this reason we use the effective frequency detuning $\tilde{\delta} = \delta - \varepsilon$, where ε corresponds to the eigenfrequency shift at the condensation threshold, see figure A1(c). For the considered parameters $\varepsilon = 1.388$.

Describing synchronization of the polariton dyad, we assume that the parameters of the model (8*a*) and (8*b*) are the same as for the case of a single condensate. This assumption is justified by the weak spatial overlap between the condensate wave functions for the inter-condensate distances considered here, see the inset to figure A1(c). The mutual coupling between spatially separated condensates, which is accounted by σ_J and σ_d parameters, affects the population and the frequency of the condensate. In particular, the steady state solutions of equations (8*a*) and (8*b*) for the symmetric and antisymmetric configurations of the polariton dyad read $|A_{\mathrm{s,as}}|^2 = |A_0|^2 \pm \sigma_\mathrm{d}/\nu$ and $\mu_{\mathrm{s,as}} = \mu_0 \pm \alpha\sigma_\mathrm{d}/\nu \pm \sigma_\mathrm{J}$, where $|A_0|^2$ and μ_0 characterize the state of a stand-alone condensate. With these solutions one can determine the dissipative σ_d and Josephson σ_J coupling parameters using the amplitude and the frequency calculated with the full model (2), see figures A1(a) and (b). In particular, at $p_0 = 4$ we get $\sigma_\mathrm{J} = 0.0292$ and $\sigma_\mathrm{d} = -0.042$.

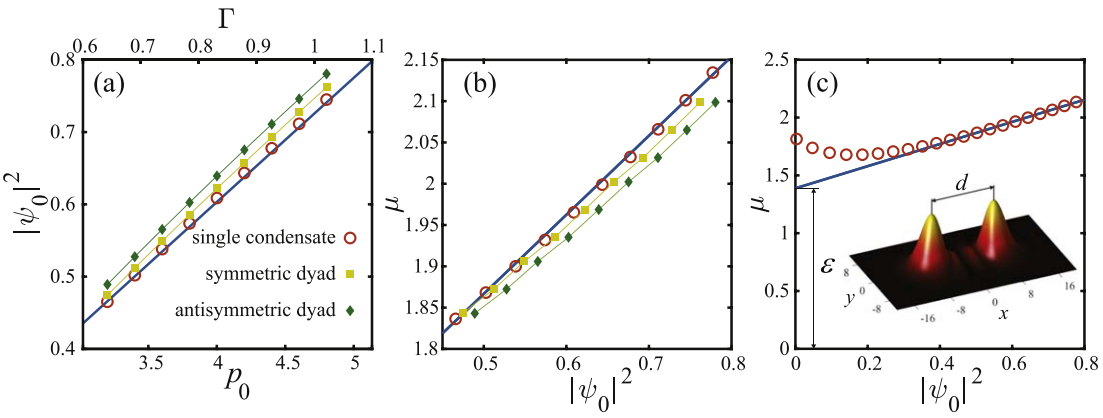

Figure A1. (a) Dependence of the condensate density maximum $|\psi_0|^2$ on the amplitude p_0 of the incoherent pump (bottom scale). The blue line shows the $|A(\Gamma)|^2$-dependence predicted by the single oscillator model (3). The corresponding values of the effective gain Γ are shown on the top scale. Red circles correspond to the properties of a single stand-alone condensate predicted by the partial differential equations model (2). Yellow squares (symmetric state) and green diamonds (antisymmetric state) correspond to the steady-state configurations of the polariton dyad in the absence of coherent pump. (b) Dependence of the frequency μ on the density maximum $|\psi_0|^2$. All markers have the same meaning as in panel (a). (c) The same as in panel (b) but for a wider range of $|\psi_0|^2$. The shift of the condensate eigenfrequency ε at the threshold ($|\psi_0|^2 = 0$) is chosen in such a way that $\mu(|A|^2)$-dependence (blue line) calculated with the model (3) fits the predictions of the full model (circles) far above the threshold. The discrepancy between the models in the vicinity of the threshold should be attributed to the depletion of the reservoir. The inset illustrates the typical shape of the polariton density distribution, $|\psi_0|^2$.

At the end of this section, we report the dimensional parameters of the main model (1*a*), (1*b*), which determine the dimensionless parameters of the normalized equations (2*a*), (2*b*): $\gamma_c = 0.5\,\mathrm{ps}^{-1}$, $\gamma_r = 0.1\,\mathrm{ps}^{-1}$, $\hbar R = 0.05\,\mu\mathrm{m}^{-2}\,\mathrm{meV}$, $g_c = 0.02\,\mu\mathrm{m}^{-2}\,\mathrm{meV}$, $g_r = 0.0175\,\mu\mathrm{m}^{-2}\,\mathrm{meV}$.

Appendix B. Normal form of the spontaneous symmetry breaking bifurcation

In this section we present the perturbation approach which reduces equations (8*a*) and (8*b*) to the normal form (9) in the vicinity of the bifurcation point $\tilde{f} = \tilde{f}_2$. It appears convenient to reformulate the problem in the vector form. The polariton state is described by $\boldsymbol{U}_i = (\Re A_1,\ \Im A_1,\ \Re A_2,\ \Im A_2)^T$ and governed by the equation

$$\partial_t \boldsymbol{U}_i = \boldsymbol{N}_i[\vec{U}] + \tilde{f}\,\boldsymbol{u}_i, \tag{B.1}$$

where $\boldsymbol{N}_i[\vec{U}]$ is a vector with components being functions of $\vec{U}$ and $\boldsymbol{u}_i = (0,\ -1,\ \ 0,\ -1)^T$. The nonlinear operator $\boldsymbol{N}_i$ is defined as

$$\boldsymbol{N}_i[\vec{U}] = M_{i,j}\boldsymbol{U}_j + \begin{pmatrix} (U_1^2 + U_1^2)(\alpha U_2 - \nu U_1) \\ (U_1^2 + U_1^2)(-\alpha U_1 - \nu U_2) \\ (U_3^2 + U_4^2)(\alpha U_4 - \nu U_3) \\ (U_3^3 + U_4^2)(-\alpha U_3 - \nu U_4) \end{pmatrix},$$

where

$$\hat{M} = \begin{pmatrix} \Gamma & -\tilde{\delta} & \sigma_\mathrm{d} & \sigma_\mathrm{J} \\ \tilde{\delta} & \Gamma & -\sigma_\mathrm{J} & \sigma_\mathrm{d} \\ \sigma_\mathrm{d} & -\sigma_\mathrm{J} & \Gamma & -\tilde{\delta} \\ \sigma_\mathrm{J} & \sigma_\mathrm{d} & \tilde{\delta} & \Gamma \end{pmatrix}.$$

Here in most cases we denote the vector quantities by bold face letters with subscripts. However, for the arguments of vector functions we use the notation of vector as an arrowed letter meaning that each of the components of the vector function depend on all components of the argument. Square brackets are used to denote the arguments of the vector functions.

A symmetric solution $A_1 = A_2 = A_\mathrm{s}$ of the equations (8*a*) and (8*b*) which is formed at $\tilde{f} > \tilde{f}_2$, is given by

$$(\mathrm{i}\Gamma + (\alpha - \mathrm{i}\nu)|A_\mathrm{s}|^2 - \tilde{\delta} + \sigma)A_\mathrm{s} = -\tilde{f}. \tag{B.2}$$

To account for the dynamics in the vicinity of the bifurcation point, we develop the perturbation theory looking for a solution in the form

$$U_i = Y_i + y_i, \tag{B.3}$$

where $Y_i[\tilde{f}] = (\Re A_s, \Im A_s, \Re A_s, \Im A_s)^T$ describes the symmetric steady state and y_i is a small perturbations of the stationary solution. To describe the steady states bifurcating from Y_i the equation for the correction has to contain the terms nonlinear in respect to y_i. We assume that the deviation from the bifurcation point $\Delta\tilde{f} = \tilde{f} - \tilde{f}_2$ is small and thus we keep only the terms linear in respect to $\Delta\tilde{f}$. Then by expansion in Taylor series we obtain

$$N_i[\vec{Y}[\tilde{f}] + \vec{y}] = N_i[\vec{Y}[\tilde{f}_2] + \vec{y}] + \frac{\partial N_i[\vec{Y}[\tilde{f}_2]]}{\partial Y_j}\frac{Y_j[\tilde{f}_2]}{\partial\tilde{f}}\Delta\tilde{f} + \frac{\partial^2 N_i[\vec{Y}[\tilde{f}_2]]}{\partial Y_j \partial Y_k}\frac{Y_j[\tilde{f}_2]}{\partial\tilde{f}}\Delta\tilde{f}\, y_k. \tag{B.4}$$

Since Y_i is a stationary solution, we have $N_i[\vec{Y}] = -\tilde{f}\, u_i$, see (B.1). This allows to transform (B.4) to

$$N_i[\vec{Y}[f] + \vec{y}] = N_i[\vec{Y}[\tilde{f}_2] + \vec{y}] - \Delta\tilde{f}\, u_i + \frac{\partial^2 N_i[\vec{Y}[\tilde{f}_2]]}{\partial Y_j \partial Y_k}\frac{Y_j[\tilde{f}_2]}{\partial\tilde{f}}\Delta\tilde{f}\, y_k. \tag{B.5}$$

Substituting (B.3) and (B.5) into (B.1) we obtain

$$\partial_t y_i = N_i[\vec{Y}[\tilde{f}_2] + \vec{y}] - N_i[\vec{Y}[\tilde{f}_2]] + \frac{\partial^2 N_i[\vec{Y}[\tilde{f}_2]]}{\partial Y_j \partial Y_k}\frac{Y_j[\tilde{f}_2]}{\partial\tilde{f}}\Delta\tilde{f}\, y_k. \tag{B.6}$$

The fact that the nonlinearity in (B.6) is cubic makes it convenient to write it in the form

$$\begin{aligned}\partial_t y_i = {} & N_{i,j,k,l}(Y_j[\tilde{f}_2] + y_j)(Y_k[\tilde{f}_2] + y_k)(Y_l[\tilde{f}_2] + y_l) \\ & - N_{i,j,k,l}Y_j[\tilde{f}_2]Y_k[\tilde{f}_2]Y_l[\tilde{f}_2] + M_{i,j}y_j + \Delta\tilde{f}\,\Lambda_{i,j}y_j,\end{aligned} \tag{B.7}$$

with

$$\Lambda_{i,j} = \frac{\partial^2 N_i[\vec{Y}[\tilde{f}_2]]}{\partial Y_j \partial Y_k}\frac{Y_k[\tilde{f}_2]}{\partial\tilde{f}}.$$

Here $N_{i,j,k,l} = \tilde{N}_{i,j,k,l} + \bar{N}_{i,j,k,l}$ accounts for the conservative part of the nonlinearity by $\tilde{N}_{i,j,k,l}$ and for the dissipative nonlinearity by $\bar{N}_{i,j,k,l}$. In the symmetric form the nonzero components of $\tilde{N}_{i,j,k,l}$ are $\tilde{N}_{1,2,2,2} = \tilde{N}_{3,4,4,4} = \alpha$, $\tilde{N}_{2,1,1,1} = \tilde{N}_{4,3,3,3} = -\alpha$, $\tilde{N}_{1,1,1,2} = \tilde{N}_{1,1,2,1} = \tilde{N}_{1,2,1,1} = \tilde{N}_{3,3,3,4} = \tilde{N}_{3,3,4,3} = \tilde{N}_{3,4,3,3} = \frac{1}{3}\alpha$, $\tilde{N}_{2,1,2,2} = \tilde{N}_{2,2,1,2} = \tilde{N}_{2,2,2,1} = \tilde{N}_{4,3,4,4} = \tilde{N}_{4,4,3,4} = \tilde{N}_{4,4,4,3} = -\frac{1}{3}\alpha$. For the nonzero components of $\bar{N}_{i,j,k,l}$ we have $\bar{N}_{1,1,1,1} = \bar{N}_{2,2,2,2} = \bar{N}_{3,3,3,3} = \bar{N}_{4,4,4,4} = -\nu$, $\bar{N}_{1,1,2,2} = \bar{N}_{1,2,1,2} = \bar{N}_{1,2,2,1} = \bar{N}_{2,1,1,2} = \bar{N}_{2,1,2,1} = \bar{N}_{2,2,1,1} = \bar{N}_{3,3,4,4} = \bar{N}_{3,4,3,4} = \bar{N}_{3,4,4,3} = \bar{N}_{4,3,3,4} = \bar{N}_{4,3,4,3} = \bar{N}_{4,4,3,3} = -\frac{1}{3}\nu$.

The operator $\hat{L}$ governing the stability of condensate state according to (B.7) is $\hat{L} = \hat{M} + 3N_{i,j,k,l}Y_kY_l + \Delta\tilde{f}\,\hat{\Lambda}$. At the point $\tilde{f} = \tilde{f}_2$ the operator $\hat{L}[\tilde{f}_2] = \hat{L}_0$ has one zero eigenvalue with an eigenvector $\boldsymbol{\xi}_i$. We scale the eigenvectors so that their norm equals 1. Then we look for the solution y_i in the form $y_i = a\boldsymbol{\xi}_i + \boldsymbol{w}_i$ where $\boldsymbol{w}_i$ is a vector orthogonal to $\boldsymbol{\xi}_i$, i.e. $(\boldsymbol{\xi}_i^\dagger, \boldsymbol{w}_i) = 0$, where the dagger symbol denotes the eigenvectors of the adjoin operators and the parenthesis with comma denote a scalar product. In this notations (B.7) takes the form

$$\begin{aligned}\boldsymbol{\xi}_i\partial_t a + \partial_t \boldsymbol{w}_i = {} & a\Delta\tilde{f}\,\Lambda_{i,j}\boldsymbol{\xi}_j + \Delta\tilde{f}\,\Lambda_{i,j}\boldsymbol{w}_j + L_{0i,j}\boldsymbol{w}_i + 3a^2N_{i,j,k,l}Y_j\boldsymbol{\xi}_k\boldsymbol{\xi}_l \\ & + 6aN_{i,j,k,l}Y_j\boldsymbol{\xi}_k\boldsymbol{w}_l + 3N_{i,j,k,l}Y_j\boldsymbol{w}_k\boldsymbol{w}_l + a^3N_{i,j,k,l}\boldsymbol{\xi}_j\boldsymbol{\xi}_k\boldsymbol{\xi}_l \\ & + 3a^2N_{i,j,k,l}\boldsymbol{\xi}_j\boldsymbol{\xi}_k\boldsymbol{w}_l + 3aN_{i,j,k,l}\boldsymbol{\xi}_j\boldsymbol{w}_k\boldsymbol{w}_l + N_{i,j,k,l}\boldsymbol{w}_j\boldsymbol{w}_k\boldsymbol{w}_l.\end{aligned} \tag{B.8}$$

In the first order approximation we obtain:

$$\partial_t a = \lambda a,$$

where $\lambda = \Delta\tilde{f}\,(\boldsymbol{\xi}_i^\dagger, \Lambda_{i,j}\boldsymbol{\xi}_j)$ corresponds to the first order approximation of the eigenvalue generating the instability. Instead of calculation of the eigenvalue perturbatively, it can be calculated solving the corresponding spectral problem. The component $\boldsymbol{w}_i$ is equal to zero in this approximation order.

Let us now find the second order contributions to a and $\boldsymbol{w}_i$. The corresponding term in the equation for a is $3a^2(\boldsymbol{\xi}_i^\dagger, N_{i,j,k,l}Y_j\boldsymbol{\xi}_k\boldsymbol{\xi}_l)\boldsymbol{\xi}_i$. This term has been evaluated numerically and it was confirmed that for the considered spontaneous symmetry breaking bifurcation this term is equal to zero up to the precision of the calculations. At the same time, the component $\boldsymbol{w}_i$ is not zero in this approximation order and has to be calculated from

$$L_{0i,j}\boldsymbol{w}_j = -3a^2(N_{i,j,k,l}Y_j\boldsymbol{\xi}_k\boldsymbol{\xi}_l - (\boldsymbol{\xi}_i^\dagger, N_{i,j,k,l}Y_j\boldsymbol{\xi}_k\boldsymbol{\xi}_l)\boldsymbol{\xi}_i).$$

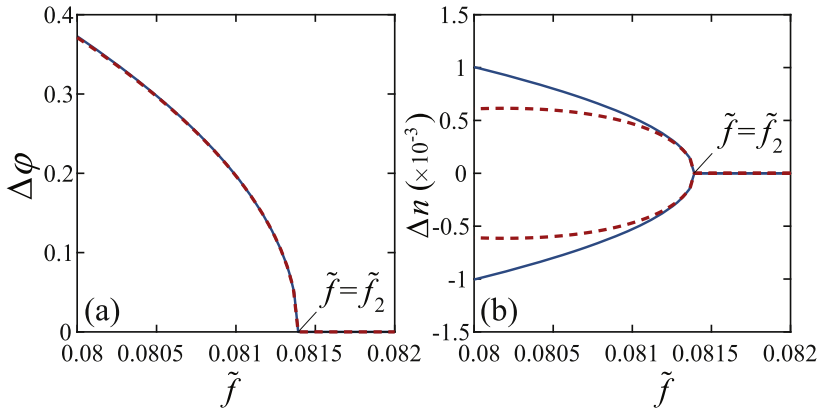

Figure B1. (a) The phase difference $\Delta\varphi$ and (b) the population imbalance Δn in the vicinity of the bifurcation point $\tilde{f} = \tilde{f}_2$. The blue curves correspond to the predictions of the two coupled oscillators model (8*a*) and (8*b*). The red curves correspond to the normal form (B.10) and (9).

The solution of this equation is

$$\boldsymbol{w}_i = -3a^2 \sum_n (\boldsymbol{\eta}_i^{(n)\dagger},\, N_{i,j,k,l} Y_j \boldsymbol{\xi}_k \boldsymbol{\xi}_l) \boldsymbol{\eta}_i^{(n)} / \lambda_n, \tag{B.9}$$

where $\boldsymbol{\eta}_i^{(n)}$ and $\boldsymbol{\eta}_i^{(n)\dagger}$ are the eigenvectors of $\hat{L}_0$ and $\hat{L}_0^{\dagger}$ corresponding to the nth nonzero eigenvalue λ_n of the operators. Let us mention, that $\partial_t \boldsymbol{w}_i$ can be neglected since characteristic time of this motion is much large than the largest inverse absolute value of λ_n.

Finally, calculation the third order terms in respect to a in (B.8) yields:

$$\partial_t a = \lambda a + \epsilon\, a^3, \tag{B.10}$$

which matches equation (9) from section 4. Here

$$\epsilon = (\boldsymbol{\xi}_i^{\dagger},\, N_{i,j,k,l} \boldsymbol{\xi}_j \boldsymbol{\xi}_k \boldsymbol{\xi}_l) + 6(\boldsymbol{\xi}_i^{\dagger},\, N_{i,j,k,l} Y_j \boldsymbol{\xi}_k \boldsymbol{w}_l).$$

Equation (B.10) is the normal form of a pitchfork bifurcation. The calculated value of ϵ for the considered system is negative. Therefore, we conclude that the spontaneous symmetry breaking occurs at the supercritical pitchfork bifurcation leading to the birth of a new stable symmetry broken states. For these states the complex amplitude of the polariton field is $a_s = \sqrt{-\epsilon/\lambda}$. Since λ depends linearly on $\tilde{f}$, we can conclude that the deviation of the symmetry broken state from the symmetric one must show a square root dependence on the detuning $\Delta\tilde{f}$ from the bifurcation point.

In order to check the validity of the perturbative approach we depict in figure B1 the phase difference $\Delta\varphi$ and the population imbalance Δn calculated with (8*a*) and (8*b*) (blue solid curves) and with the normal form equation (B.10) (red dashed curves). An excellent coincidence in the vicinity of the bifurcation point justifies the developed perturbation theory.

Appendix C. The analysis of the synchronization scenario in terms of the coupled phase oscillators model

Here we aim to find stationary solutions of (10) and analyze their stability. Only the stable stationary state provides synchronization of the polariton dyad to the coherent laser light. It is convenient to rewrite (10) in the form

$$\partial_t \phi = \sin\phi (f' \cos\theta - 2\sigma_{\mathrm{d}} \cos\phi), \tag{C.1}$$

$$\partial_t \theta = q - \sigma_{\mathrm{J}} \cos 2\phi + f' \sin\theta \cos\phi, \tag{C.2}$$

where $\phi = (\varphi_2 - \varphi_1)/2$ and $\theta = (\varphi_2 + \varphi_1)/2 - \pi/2$.

The symmetric stationary states implies $\sin\phi = 0$. Hence according to (C.2) there are four independent symmetric solutions:

$$\phi = 0, \quad \theta = -\arcsin\left(\frac{q - \sigma_{\mathrm{J}}}{f'}\right), \tag{C.3}$$

$$\phi = 0, \quad \theta = \pi + \arcsin\left(\frac{q-\sigma_J}{f'}\right), \tag{C.4}$$

$$\phi = \pi, \quad \theta = \arcsin\left(\frac{q-\sigma_J}{f'}\right), \tag{C.5}$$

$$\phi = \pi, \quad \theta = \pi - \arcsin\left(\frac{q-\sigma_J}{f'}\right), \tag{C.6}$$

which exist at $f' > |q-\sigma_J|$, see condition (14) in the main text.

The states with broken symmetry appear provided that the expression in parenthesis in (C.1) vanishes, i.e. at

$$\cos\phi = (f'/2\sigma_d)\cos\theta. \tag{C.7}$$

Substituting this expression to (C.2) one obtains four pairs of the symmetry broken states:

$$\theta = -\frac{1}{2}(\chi + \arcsin B), \tag{C.8}$$

$$\theta = -\frac{1}{2}(\chi + \arcsin B) + \pi, \tag{C.9}$$

$$\theta = -\frac{1}{2}(\chi - \arcsin B) + \frac{\pi}{2}, \tag{C.10}$$

$$\theta = -\frac{1}{2}(\chi - \arcsin B) - \frac{\pi}{2}, \tag{C.11}$$

where $\chi = -\arcsin\left(\frac{\sigma_J/\sigma_d}{\sqrt{1+\sigma_J^2/\sigma_d^2}}\right)$ and $B = \frac{4\sigma_d(q+\sigma_J(1-f'^2/4\sigma_d^2))}{f'^2\sqrt{1+\sigma_J^2/\sigma_d^2}}$. For each value of θ there are two states with $\phi = \pm\arccos((f'/2\sigma_d)\cos\theta)$.

Solutions (C.8)–(C.11) require $B \leqslant 1$. This condition is satisfied provided that the coherent pumping strength exceeds the critical value defined by the following equation:

$$f'^4 + 8f'^2\sigma_J(q+\sigma_J) - 16\sigma_d^2(q+\sigma_J)^2 = 0, \tag{C.12}$$

which has only one real root given by (11) in the main text.

Besides, (C.7) imposes an additional condition on the existence of the symmetry broken states, namely, $(f'^2/4\sigma_d^2)\cos^2\theta \leqslant 1$. Then, expressing $\cos^2\theta$ from (C.2), one obtains

$$D \pm \sqrt{D^2 - 16(q+\sigma_J)^2(\sigma_J^2+\sigma_d^2)} \leqslant 8(\sigma_J^2+\sigma_d^2), \tag{C.13}$$

where $D = f'^2 + 4\sigma_J(q+\sigma_J)$. A plus sign in (C.13) corresponds to the states (C.8) and (C.9) while minus stands for (C.10) and (C.11). In the former case (C.13) satisfies provided that the conditions

$$f' \leqslant \sqrt{4\sigma_d^2 + (q-\sigma_J)^2} \tag{C.14}$$

and

$$f'^2 \leqslant 8(\sigma_J^2+\sigma_d^2) - 4\sigma_J(q+\sigma_J) \tag{C.15}$$

are satisfied simultaneously. Equation (C.14) defines the position of the pitchfork symmetry breaking bifurcation, see (13) in the main text. Expressing q from (C.14) and (C.15), one obtains the range of detuning (12) where the states (C.8) and (C.9) exist.

The states (C.10) and (C.11) exist where either (C.15) holds or

$$f' \geqslant \sqrt{4\sigma_d^2 + (q-\sigma_J)^2}. \tag{C.16}$$

This domain corresponds to the region on the right from the green curve in figure 4.

The stability analysis of the stationary solutions implies their perturbation in the form $\phi = \phi_0 + \delta\phi\exp(\mu^{(L)}t)$ and $\theta = \theta_0 + \delta\theta\exp(\mu^{(L)}t)$, where ϕ_0 and θ_0 correspond to the stationary states and $\delta\phi$, $\delta\theta$ are small perturbations. From (C.1) and (C.2) for the Lyapunov exponent $\mu^{(L)}$ we obtain

$$\mu_{1,2}^{(L)} = -\sigma_d\cos 2\phi_0 + f'\cos\phi_0\cos\theta_0 \pm (\sigma_d^2\cos^2 2\phi_0 - \sigma_J^2\sin^2 2\phi_0 + (f'\sin\phi_0\sin\theta_0 - \sigma_J\sin 2\phi_0)^2)^{1/2}. \tag{C.17}$$

For the symmetric solutions:

$$\mu_{1,2}^{(L)} = -\sigma_d \pm |\sigma_d| + f'\cos\phi_0\cos\theta_0. \tag{C.18}$$

For the states (C.3) and (C.6) the last term in (C.18) is positive. Thus these solutions are unstable, $\mu_{1,2}^{(L)} > 0$, at any sign of the dissipative coupling. In contrast, the states (C.4) and (C.5) are always stable at $\sigma_d > 0$. However in the

opposite case $\sigma_{\rm d} < 0$, which corresponds to the synchronization of the antisymmetric dyad, they become stable only where the condition (C.16) is satisfied.

For the symmetry broken solutions (C.8)–(C.11) the Lyapunov exponents are

$$\mu_{1,2}^{(\rm L)} = \sigma_{\rm d} \pm (\sigma_{\rm d}^2 \cos^2 2\phi_0 + f'^2 \sin^2\phi_0 \sin^2\theta_0 - 4\sigma_{\rm J} f' \sin^2\phi_0 \cos\phi_0 \sin\theta_0)^{1/2}. \tag{C.19}$$

At $\sigma_{\rm d} > 0$ the stability problem eigenvalue (C.19) is always positive. Thus, the symmetric dyad can not be synchronized in the symmetry broken state. In the opposite case ($\sigma_{\rm d} < 0$), $\mu_2^{(\rm L)} < 0$ always, while the first exponent vanishes, $\mu_1^{(\rm L)} = 0$, at $\cos\phi_0 = 1$. The latter condition determines the boundary of the existence domain of the symmetry broken states, see (C.13). The analysis demonstrates that the states (C.8) and (C.9) remain stable in the domain of their existence, while the states (C.10) and (C.11), on the contrary, are always unstable.

ORCID iDs

I Y Chestnov https://orcid.org/0000-0002-3949-5421

References

[1] Weisbuch C, Nishioka M, Ishikawa A and Arakawa Y 1992 *Phys. Rev. Lett.* **69** 3314
[2] Christopoulos S *et al* 2007 *Phys. Rev. Lett.* **98** 126405
[3] Su R, Wang J, Zhao J, Xing J, Zhao W, Diederichs C, Liew T C H and Xiong Q 2018 *Sci. Adv.* **4** eaau0244
[4] Schneider C *et al* 2013 *Nature* **497** 348
[5] Kasprzak J *et al* 2006 *Nature* **443** 409
[6] Sun Y, Wen P, Yoon Y, Liu G, Steger M, Pfeiffer L N, West K, Snoke D W and Nelson K A 2017 *Phys. Rev. Lett.* **118** 016602
[7] Baas A, Lagoudakis K G, Richard M, André R, Dang L S and Deveaud-Plédran B 2008 *Phys. Rev. Lett.* **100** 170401
[8] Wouters M 2008 *Phys. Rev.* B **77** 121302
[9] Ohadi H, Gregory R L, Freegarde T, Rubo Y G, Kavokin A V, Berloff N G and Lagoudakis P G 2016 *Phys. Rev.* X **6** 031032
[10] Ohadi H, Dreismann A, Rubo Y G, Pinsker F, del Valle-Inclan Redondo Y, Tsintzos S, Hatzopoulos Z, Savvidis P and Baumberg J J 2015 *Phys. Rev.* X **5** 031002
[11] Aleiner I L, Altshuler B L and Rubo Y G 2012 *Phys. Rev.* B **85** 121301
[12] Kalinin K P and Berloff N G 2018 *New J. Phys.* **20** 113023
[13] Berloff N G, Silva M, Kalinin K, Askitopoulos A, Töpfer J D, Cilibrizzi P, Langbein W and Lagoudakis P G 2017 *Nat. Mater.* **16** 1120
[14] Lagoudakis P G and Berloff N G 2017 *New J. Phys.* **19** 125008
[15] Nixon M, Fridman M, Ronen E, Friesem A A, Davidson N and Kanter I 2012 *Phys. Rev. Lett.* **108** 214101
[16] Jang J K, Klenner A, Ji X, Okawachi Y, Lipson M and Gaeta A L 2018 *Nat. Photon.* **12** 688
[17] Kalinin K P and Berloff N G 2018 *Phys. Rev. Lett.* **121** 235302
[18] Caputo D, Bobrovska N, Ballarini D, Matuszewski M, De Giorgi M, Dominici L, West K, Pfeiffer L N, Gigli G and Sanvitto D 2019 *Nat. Photon.* **13** 488
[19] Pikovsky A, Rosenblum M and Kurths J 2003 *Synchronization: A Universal Concept in Nonlinear Sciences* (Cambridge: Cambridge University Press)
[20] Wouters M and Carusotto I 2007 *Phys. Rev. Lett.* **99** 140402
[21] Baas A, Karr J P, Eleuch H and Giacobino E 2004 *Phys. Rev.* A **69** 023809
[22] Kalinin K P, Lagoudakis P G and Berloff N G 2018 *Phys. Rev.* B **97** 094512
[23] Sakaguchi H, Malomed B A and Skryabin D V 2017 *New J. Phys.* **19** 085003